

Article

# A Pitch Angle Controller Based on Novel Fuzzy-PI Control for Wind Turbine Load Reduction

Bofeng Xu <sup>1,\*</sup>, Yue Yuan <sup>1</sup>, Haoming Liu <sup>1</sup> , Peng Jiang <sup>1,2</sup>, Ziqi Gao <sup>2</sup>, Xiang Shen <sup>3</sup> and Xin Cai <sup>4</sup>

<sup>1</sup> Research Center for Renewable Energy Generation Engineering of Ministry of Education, Hohai University, Nanjing 211100, China; yyuan@hhu.edu.cn (Y.Y.); liuhaom@hhu.edu.cn (H.L.); jiangpeng@c.ccs.org.cn (P.J.)

<sup>2</sup> Goldwind Science & Technology Co., Ltd., Beijing 100176, China; gaoziqi@goldwind.com.cn

<sup>3</sup> Department of Mechanical and Construction Engineering, Northumbria University, Newcastle upon Tyne NE1 8ST, UK; shaun.shen@northumbria.ac.uk

<sup>4</sup> Jiangsu Province Wind Power Structural Engineering Research Center, Hohai University, Nanjing 211100, China; xcai@hhu.edu.cn

\* Correspondence: bfxu1985@hhu.edu.cn

Received: 15 September 2020; Accepted: 16 November 2020; Published: 20 November 2020



**Abstract:** A novel fuzzy rule is proposed to adopt a positive pitch strategy when the error between the measured and rated generator speed becomes large and continues to increase, and to adopt a negative pitch strategy when the error is small. The improved approach is introduced into the normal Fuzzy-Proportional-Integral (Fuzzy-PI) control strategy by dividing the fuzzy rules into four areas and analyzing the design method for each area. Furthermore, a low pass filter is used to reduce the ultimate loads of the pitch driver caused by the novel fuzzy rules. The modeling of the wind turbine load under turbulent wind conditions is conducted in GH Bladed, and MATLAB/Simulink is used to interact with the modeling to verify the novel Fuzzy-PI control. The results show that, compared with normal Fuzzy-PI control, the novel Fuzzy-PI control can greatly reduce the ultimate loads and fatigue loads of the pitch driver. The novel Fuzzy-PI control not only reduces the extremum of power deviation, but also decreases some ultimate loads and fatigue loads of the tower base and the blade root. It can reduce these loads by up to 21.53% under the normal turbulent wind condition and by up to 18.14% under the extreme turbulent wind condition.

**Keywords:** wind turbine; fuzzy rules; Fuzzy-PI control; load reduction; pitch angle controller

## 1. Introduction

Wind power has been developing rapidly worldwide due to fossil fuel energy depletion and environmental pollution. In recent years, the horizontal axis wind turbine (HAWT), especially on large-scale HAWT, has taken much of the wind energy market because of its high efficiency of harvesting wind energy. However, the growing need for higher power generation per turbine makes the size of HAWT, both in terms of the blade length and tower height, increase rapidly [1]. When facing complex atmospheric conditions, the elimination or mitigation of excessive loads for modern large-scale turbines is very necessary because it not only lessens the manufacture cost of turbines by reducing design requirements but also extends the life of wind turbine key components [2].

Challenges of the controller design in wind turbines are introduced by the large moment of inertia and nonlinearity of wind turbines [3], along with random natural wind speeds with wide variation ranges. Traditional pitch angle controllers were normally based on proportional integral derivative (PID) control. Although PID has a simple structure and high reliability, its parameters are fixed and cannot meet the multiple time-varying and nonlinear characteristics of wind turbines. However, fuzzy control technology is based on fuzzy reasoning and linguistic rules; hence, the influence of the

nonlinear factors can be avoided [4]. Moreover, compared with the ordinary PID pitch angle controller, fuzzy logic control (FLC) can reduce the fluctuation of the torque and power of the drive system [5,6]. Han [5] and Civelek [7] combined FLC with individual pitch angle control to further reduce the loads of the tower base and the blade root. Fuzzy self-tuning PID (Fuzzy-PID) control [8,9] has been proposed to simultaneously exert better control on the FLC in nonlinear systems and higher reliability on the ordinary PID control. Compared with the ordinary PI control, Fuzzy-PID control can effectively reduce the overshoot of the pitch angle, increase system response speed, and stabilize the output power of the wind turbines [10,11]. In addition, compared with FLC, these advantages of Fuzzy-PI control will decrease slightly, but remain [12,13]. All in all, these literatures have verified the Fuzzy-PI control in wind turbine control. On the other hand, some statistical approaches have been used to promote the performance and efficiency of energy systems, for example in solar collector applications [14–16].

Little attention has been paid to the design method of fuzzy rules and the variation of wind turbine loads although it is critical for designing and estimating Fuzzy-PID control. This study compared normal and extreme turbulent wind conditions with odd wind conditions, such as step down and step up in wind speed, presenting better similarity to natural wind conditions and better validating performance on control algorithms. Moreover, the improved approach is introduced into the normal Fuzzy-PI control strategy by dividing the fuzzy rules into four areas and analyzing the design method for each area. Wind turbine performance under normal and extreme turbulent wind conditions was simulated in GH Bladed and MATLAB/Simulink interactive software, and the variation of wind turbine loads was analyzed.

## 2. Wind Turbine Model

### 2.1. Aerodynamic Model

Wind turbines capture energy through rotating blades, and the captured energy is then transferred through the shaft to the generator in the form of torque to generate electricity. The relationship between power and wind speed can be expressed as follows [17]:

$$P_a = \frac{1}{2} C_p(\lambda, \beta) \rho R^2 \pi v^3 \quad (1)$$

$$\lambda = \frac{\omega R}{v} \quad (2)$$

where  $P_a$  is the aerodynamic power captured by wind turbine's rotor blades,  $C_p$  is the rotor power coefficient,  $\rho$  is the density of air,  $R$  is the rotation radius of the blade,  $v$  is the wind speed,  $\lambda$  is the tip-speed ratio, and  $\beta$  is the pitch angle of the blade. Generally, the rotor power coefficient  $C_p$  can be approximately described as follows:

$$C_p(\lambda, \beta) = 0.5176 \left( \frac{116}{\lambda_i} - 0.4\beta - 5 \right) e^{-\frac{21}{\lambda_i}} + 0.0068\lambda \quad (3)$$

$$\frac{1}{\lambda_i} = \frac{1}{\lambda + 0.08\beta} - \frac{0.035}{\beta^3 + 1} \quad (4)$$

### 2.2. Drive Train Model

The drive system of wind turbines is mainly composed of a wind rotor, low speed shaft, gear box, high speed shaft, and generator rotor. In this paper, a common two-mass flexible axis model, the force diagram of which is illustrated in Figure 1, is selected. The model considers that the low-speed and high-speed shafts are flexible, which allows the rotor of the wind turbine and the generator to have their own rotational degrees of freedom. The acceleration of the rotor is determined by the imbalance between the aerodynamic torque and the braking torque of the low-speed shaft, and the acceleration of

the generator rotor is determined by the imbalance between the high-speed shaft drive torque and the generator torque.

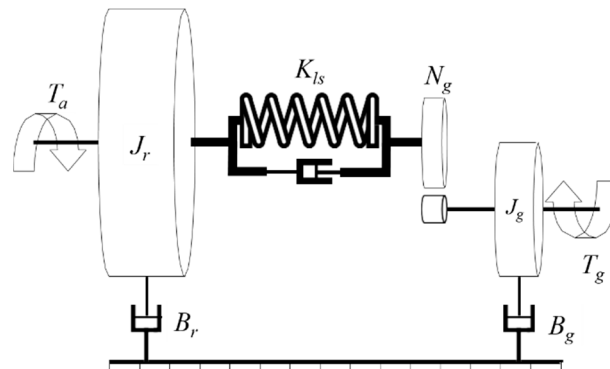


**Figure 1.** Two-mass flexible shaft drive train model.

The rotor shaft equation can be derived as follows:

$$J_r \frac{d\omega_r}{dt} = T_a - T_{ls} - B_r \omega_r \quad (5)$$

$$T_{ls} = K_{ls}(\theta_r - \theta_{ls}) + B_{ls}(\omega_r - \omega_{ls}) \quad (6)$$

where  $J$  is the second moment of inertia,  $B$  is the damping coefficient,  $K$  is the spring constant,  $T$  is the torque,  $\theta$  is the shaft angular displacement, and  $\omega$  is the shaft angular speed. The subscripts  $r$ ,  $ls$ , and  $a$  denote the rotor, low speed, and applied by blades, respectively. On the generator side, it is considered to be:

$$J_g \frac{d\omega_g}{dt} = T_{hs} - T_g - B_g \omega_g \quad (7)$$

where the subscripts  $hs$  and  $g$  denote high speed and the generator, respectively.

In this paper, the gearbox is considered ideal with no loss, as follows:

$$N_g = \frac{T_{ls}}{T_{hs}} = \frac{\omega_g}{\omega_{ls}} \quad (8)$$

where  $N_g$  is the gearbox ratio.

### 2.3. Generator Model

Since the main focus of this paper is on designing pitch angle controller and for purpose of simplicity, a first-order model [18] for the generator is considered as follows:

$$\frac{dT_g}{dt} = \frac{1}{\tau_g}(T_{ref} - T_g) \quad (9)$$

where  $\tau_g$  is the time constant of the generator, and  $T_{ref}$  is the generator's torque reference. The captured electrical power [19] is equal to:

$$P_g = \eta_g \cdot \omega_g \cdot T_g \quad (10)$$

where  $\eta_g$  is the generator efficiency.

### 2.4. Pitch Actuator Model

The pitch actuator provides the rotational movement of each blade of the wind turbine around its longitudinal axis. It is modeled as an underdamped hydraulic mechanism, which is more reliable with

little backlash and larger stiffness than the electrical pitch actuator motor [20,21]. The hydraulic pitch actuator is thus described as a second order dynamic system as:

$$\frac{d^2\beta}{dt^2} = -\omega_n^2\beta - 2\omega_n\xi\frac{d\beta}{dt} + \omega_n^2\beta_{ref} \quad (11)$$

where,  $\omega_n$  and  $\xi$  are the natural frequency and damping ratio of the pitch actuator, respectively. Additionally,  $\beta_{ref}$  is the reference pitch angle, commanded by the pitch controller and to be followed by blade pitch angle.

The speed of wind turbines has a rated value which is limited by the loads that the wind turbine material can bear. Due to the voltage and current resistance of power electronic components, the output power of wind turbines also has a rated value. Combined with (1)–(8), in order to limit the rising speed and power, the blade angle must be increased when the wind speed increases continuously. Wind turbine pitch actuators usually have two important limitations in amplitude and pitch angle rate of change. In this paper, the amplitude and rate limitation are considered between  $0^\circ$  up to  $90^\circ$  and  $-8^\circ/s$  up to  $+8^\circ/s$  [22], respectively.

### 3. Fuzzy-PID Control Algorithm

#### 3.1. Fuzzy Logic Control Algorithm

The work of fuzzy control is mainly divided into three processes: fuzzification, fuzzy logic reasoning, and defuzzification [23,24]. In the process of fuzzification, the exact input is converted into the form of a fuzzy set and a membership function for fuzzy reasoning. In general, the fuzzy variables are divided into the following: {negative large, negative medium, negative small, zero, positive small, positive middle, and positive large}, the shorthand representations of which are {NL, NM, NS, ZO, PS, PM, and PL}. Fuzzy logic reasoning is the core component of FLC, which is responsible for the output of fuzzification according to the knowledge of the rules and databases. The process of defuzzification transforms the fuzzy variables obtained from fuzzy logic reasoning into precision output parameters applied to the controlled equipment. According to the existing literature [25], the central average method is the best method. The output control value fed into the system is calculated by the following formula:

$$y = \frac{\sum_j \delta_j \mu_j}{\sum_j \mu_j} \quad (12)$$

where  $\delta$  is the center of the fuzzy output set,  $\mu$  is the height of the fuzzy output set, and  $y$  is the output of the control. The subscript  $j$  denotes the  $j$ -th time.

#### 3.2. Fuzzy-PID Control Algorithm

As sampling control, computer control calculates the controlled value according to the deviation value of the sampling time. The assumption is that the sampling interval is  $T$ , and the error and the derivative of the error are, respectively, denoted as  $e$  and  $e'$ . The input deviation and PID output [26] at the  $k$ -th time sampling are:

$$e(k) = y_{ref}(k) - y(k) \quad (13)$$

$$e'(k) = \frac{e(k) - e(k-1)}{T} \quad (14)$$

$$y(k) = P(k) + I(k) + D(k) \quad (15)$$

$$P(k) = k_p \cdot e(k) \quad (16)$$

$$I(k) = k_i \cdot \sum_{j=0}^k [e(j) \cdot T] \tag{17}$$

$$D(k) = k_d \cdot e'(k) \tag{18}$$

where  $y_{ref}$  is the set value,  $y$  is the actual output value,  $k_p$  is the proportional gain,  $k_i$  is the integral gain,  $k_d$  is the differential gain,  $P$  is the proportional output item,  $I$  is the integral output item, and  $D$  is the differential output item.

According to the input value, the Fuzzy-PID control strategy modifies the proportional, integral, and differential gain coefficients in real time to achieve a better control effect. The block diagram of the Fuzzy-PID control strategy system based on two-dimensional FLC theory is illustrated in Figure 2.

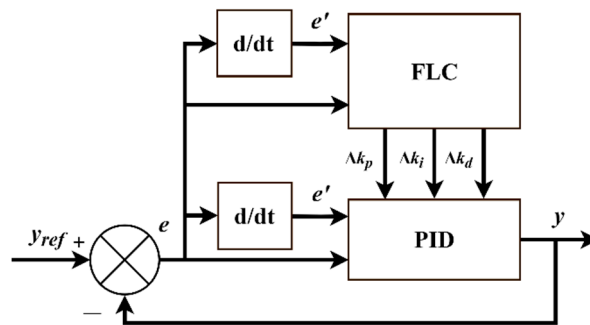


Figure 2. Block diagram of Fuzzy-PID control strategy system.

#### 4. Design of Simulation Platform and Fuzzy Rules

##### 4.1. Design of GH Bladed and MATLAB/Simulink Interactive Software

The design of GH Bladed and MATLAB/Simulink interactive software was supported by MATLAB Engine technology [27] and Named Pipes technology [28]. MATLAB Engine technology is one of the interface programs provided by MATLAB, whose technology supports C/C++ and other types of programming. Through this, users are able to apply a single script to call all functions supported by MATLAB to achieve the data interaction between software and MATLAB. The data interaction between interactive software and DLL files can be realized by using the Named Pipes technology, which can interact the data between different processes of the same computer. The flow of interactive software data (arrow direction) is shown in Figure 3.

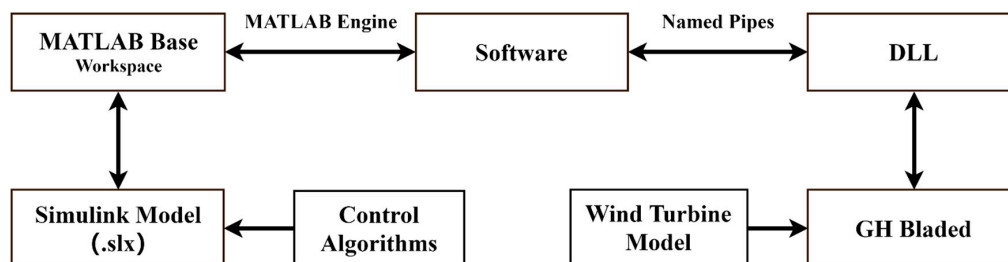


Figure 3. Data flow diagram of interactive software.

##### 4.2. Improvement of Fuzzy Rules

The PI control is generally adopted in industry, and (15), (16), and (17), respectively, become (19), (20), and (21). Based on the GH Bladed and MATLAB/Simulink interactive software, the Fuzzy-PID model was constructed in this work in Simulink, as shown in Figure 4.

$$y(k) = P(k) + I(k) \tag{19}$$

$$P(k) = (k_{p0} + \Delta k_p) \cdot e(k) \tag{20}$$

$$I(k) = I(k - 1) + (k_{i0} + \Delta k_i) \cdot e(k) \tag{21}$$

where  $k_{p0}$  is the initial proportional gain,  $k_{i0}$  is the initial integral gain,  $\Delta k_p$  is the variability of the proportional gain of the FLC output, and  $\Delta k_i$  is the variability of the integral gain of the FLC output.

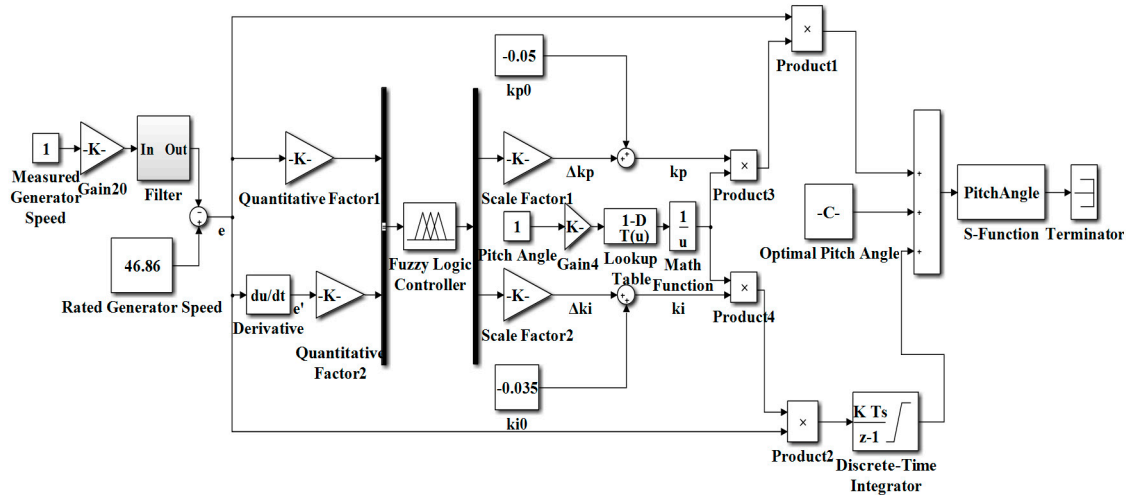


Figure 4. Block diagram of Fuzzy-PI control Simulink.

The linearized model of wind turbines at rated wind speed is determined by using the linearized module of GH Bladed, while the parameters of PI control ( $k_{p0} = -0.05$ ,  $k_{i0} = -0.035$ ) are found using the 4:1 attenuation curve method [29]. Considering the nonlinearity of wind turbines, the proportional and integral gains are adjusted in real time according to the pitch angle [26]. The fuzzy rules according to the existing literature [12,13] are listed in Table 1.

Table 1. Fuzzy rules.

$\Delta k_p / \Delta k_i$	$e'$							
	NL	NM	NS	ZO	PS	PM	PL	
$e$	NL	NL	NM	NS	PS	PS	PM	PL
	NM	NL	NM	NS	PS	PS	PM	PL
	NS	NL	NM	NS	ZO	PS	PM	PL
	ZO	PL	PM	PS	ZO	NS	NM	NL
	PS	PL	PM	PS	ZO	NS	NM	NL
	PM	PL	PM	PS	NS	NS	NM	NL
	PL	PL	PM	PS	NS	NS	NM	NL

To facilitate the analysis and design of the fuzzy rules, this paper divides the rules into four areas, as shown in Figure 5. Taking a measured generator speed that is greater than the rated speed as an example ( $e$  is negative), the design ideas of areas 1, 2, 3, and 4 in the upper parts of the fuzzy rules table are described below. In area 1, at this time, the speed deviation  $e$  and its derivative  $e'$  are both less than zero, which indicates that the speed of the wind turbines will further increase. To control the deterioration of the speed, an actively variable pitch strategy is adopted to restrain the ultimate loads of the wind turbines. Due to this, the fuzzy rules of area 1 were set as presented in Table 1.

Some of the goals of the control algorithms of wind turbines are the speed and accuracy of calculations. However, the strong nonlinearity of wind turbines makes it impossible to establish an accurate model [30], so the control algorithms cannot obtain accurate results. In addition, the rapid changes of wind speed and the tower vibration [31] make a very high demand on the computation speed. Moreover, the pitch actuator’s mechanical delay of hundreds of milliseconds [32] prevents the

controller’s signal from being executed immediately. These problems result in inevitable overshoot. Equation (21) indicates that, in this case ( $e$  is negative), if overshoot occurs in the integral output, a positive deviation  $e$  is needed to correct the overshoot. In addition, the demand is opposite to the truth and the rotor speed will be faster which is obviously not conducive to the stability of wind turbines. However, according to (5)–(8), if the pitch angle overturns,  $e'$  will become positive. Considering the influence of factors such as the actuator’s mechanical delay and tower vibration, the values of  $k_p$  and  $k_i$  are increased to avoid overturns in area 3, which is different from Table 1.

		$e'$					
		NL	NM	NS	ZO	PS	PM
$e$	NL						
	NM	1		3		2	
	NS						
	ZO	4					
	PS						
	PM	2		3		1	
	PL						

Figure 5. Partition diagram of fuzzy rules.

In area 2, the pitch angle is too large, and the rotor speed of the wind turbines decreases rapidly. As the output of Fuzzy-PI control is determined by both proportional and integral output items, the value of  $k_i$  is increased (approaching 0) at this time to maintain the integral output item, and the value of  $k_p$  is increased to reduce the proportional output; this solves the problem of overshoot of the pitch angle. Equation (21) indicates that if overshoot occurs in the integral output, a positive deviation  $e$  is needed to correct the overshoot. The values of  $\Delta k_i$  in area 2 were set to be larger than those in Table 1 to avoid this condition. Meanwhile, referring to (1)–(8) and (19)–(21), the rapid increase in the values of  $\Delta k_p$  may result in a further increase in rotor speed and pitch rate, which will lead to large ultimate loads of the pitch driver. Therefore, the values of  $\Delta k_p$  in area 2 were set as smaller than those in Table 1.

As mentioned previously, the strong nonlinearity of the wind turbine, the rapid changes of wind speed, the tower vibration, and the actuator’s mechanical delay make it impossible to achieve an accurate pitch angle. In industry, the deviation rate of the speed and output power is allowed to fluctuate within the range of 5% [33], which corresponds to area 4 in the fuzzy rules table. For this area, this paper adopts a negative control strategy of variable pitch, which can not only ensure the speed deviation and output power of wind turbines within a reasonable range, but also effectively reduces the fatigue loads of the pitch driver. According to (21), to reduce the change of the integral output item, only the value of  $k_i$  needs to be appropriately increased. However, according to (20), the proportional output item can mutate. Therefore, the variable  $k_{p2}$  was creatively introduced in this work, and determines the proportional output item by judging the size of  $k_{p2}$ . Equation (20) thus becomes (22).

$$P(k) = \begin{cases} P(k-1), k_{p2} < 0 \\ (k_{p0} + \Delta k_p) \cdot e(k), k_{p2} \geq 0 \end{cases} \quad (22)$$

However, according to (22), when the wind turbine state transfers from area 4 to other areas, the proportional output term may change abruptly, which will greatly increase the ultimate loads of the pitch driver. Therefore, a low pass filter is added after the proportional output item to achieve smooth transition. So far, the fuzzy rules achieve the following: when the rotation speed deviation is large and will continue to increase, an actively variable pitch strategy is adopted to restrain the ultimate loads of wind turbines; when the speed deviation is relatively small, the fatigue loads of the pitch driver are reduced by adopting a negatively variable strategy under the condition that the rotation speed

deviation is within the limited range. This design idea is also applicable when the measured generator speed is smaller than the rated speed ( $e$  is positive), and all the novel fuzzy rules are presented in Table 2.

**Table 2.** Novel fuzzy rules.

$\Delta k_p$		$e'$						
		NL	NM	NS	ZO	PS	PM	PL
$e$	NL	NL	NM	NS	NS	NS	NS	ZO
	NM	NL	NM	NS	NS	NS	ZO	PS
	NS	NM	NS	ZO	ZO	ZO	ZO	PS
	ZO	$k_{p2}$						
	PS	PS	ZO	ZO	ZO	ZO	NS	NM
	PM	PS	ZO	NS	NS	NS	NM	NL
	PL	ZO	NS	NS	NS	NS	NM	NL
$\Delta k_i$		$e'$						
		NL	NM	NS	ZO	PS	PM	PL
$e$	NL	NL	NM	PL	PL	PL	PL	PL
	NM	NL	NM	PL	PL	PL	PL	PL
	NS	NM	NM	PL	PL	PL	PL	PL
	ZO	PS						
	PS	PL	PL	PL	PL	PL	NM	NM
	PM	PL	PL	PL	PL	PL	NM	NL
	PL	PL	PL	PL	PL	PL	NM	NL
$k_{p2}$		$e'$						
		NL	NM	NS	ZO	PS	PM	PL
$e$	NL	PL						
	NM	PL						
	NS	PL						
	ZO	NL						
	PS	PL						
	PM	PL						
	PL	PL	PL	PL	PL	PL	PL	PL

## 5. Simulation and Loads Analysis

### 5.1. Information of Wind Turbine, Wind Model, and Loads

Some parameters of the 2 MW medium-speed permanent magnet wind turbine used for simulation are listed in Table 3.

**Table 3.** Wind turbine parameters.

Parameter	Value
Rated power (KW)	2000
Rated speed of wind rotor ( $r \cdot \min^{-1}$ )	11.81
Diameter of wind rotor (m)	130.62
Power regulation mode	Variable speed and variable blade
Variable drive mode	Hydraulic drive
Cut-in speed ( $m \cdot s^{-1}$ )	3
Cut-out speed ( $m \cdot s^{-1}$ )	19
Rated speed ( $m \cdot s^{-1}$ )	8.4

GH Bladed provides two wind models, namely the von Karman [34] and the Kaimal models [35]. Both models are generally accepted as good representations of real atmospheric turbulence, although

they use slightly different forms for the auto-spectral and cross-spectral density functions. The Kaimal model was selected for the simulations in the present study. A three-component Kaimal model has been introduced for compatibility with the IEC-61400-1 [36]. The auto-spectral density for the longitudinal ( $i = u$ ), lateral ( $i = v$ ), and vertical ( $i = w$ ) components of turbulence, according to the Kaimal model, is:

$$\frac{n \cdot S_{ii}(n)}{\sigma_i^2} = \frac{4n_i}{(1 + 6n_i)^{5/3}} \quad (i = u, v, w) \quad (23)$$

where  $S_{ii}$  is the auto-spectrum of wind speed variation,  $n$  is the frequency of variation,  $\sigma_i$  is the standard deviation of wind speed variation, and  $n_i$  is a nondimensional frequency parameter [35].

The external conditions to be considered for design are dependent on the intended site or site type for a wind turbine installation. Wind turbine classes are defined in terms of wind speed and turbulence parameters. The values of wind speed and turbulence parameters are intended to represent many different sites, and do not give a precise representation of any specific site. The wind turbine classification offers a range of robustness clearly defined in terms of the wind speed and turbulence parameters [36]. The class of the wind turbine used for simulation is IIB, which means that the expected value of hub-height turbulence intensity at a 10 min average wind speed of 15 m/s ( $I_{ref}$ ) is 0.14, and the reference wind speed of the hub height ( $V_{ref}$ ) is 42.5 m/s. The standard deviation of longitudinal variation in normal and extreme turbulent wind conditions for hub height ( $\sigma_u$ ) are provided by (24) and (25):

$$\sigma_u = I_{ref}(0.75V_{hub} + 5.6) \quad (24)$$

$$\sigma_u = 2I_{ref}\left(0.072\left(\frac{0.2V_{ref}}{2} + 3\right)\left(\frac{V_{hub}}{2} - 4\right) + 10\right) \quad (25)$$

where  $V_{hub}$  is the average wind speed of the hub height.

The standard deviations of lateral variation and vertical variation are given by (26) and (27).

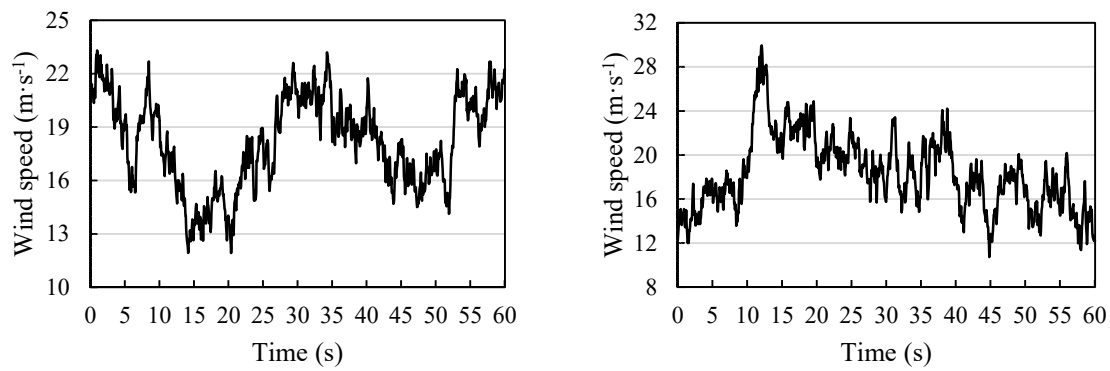
$$\sigma_v = 0.7\sigma_u \quad (26)$$

$$\sigma_w = 0.5\sigma_u \quad (27)$$

Referring to (1)–(8), to study the influence of the pitch angle controller based on novel Fuzzy-PI control on wind turbine loads and power, the simulation wind speed was set as greater than the rated wind speed, and the torque was set to the rating to eliminate its interference. The average wind speed of the hub height was set as  $18 \text{ m}\cdot\text{s}^{-1}$ , and the GH Bladed software was used to generate the wind data of normal and extreme turbulent wind conditions, which are presented in Figure 6. According to International Standard IEC 61400-1, the expected value of the turbulence intensity at the reference wind speed 15 m/s is 0.14, and the turbulence intensity is 13.22%.

In this study, more attention is paid to the loads of the tower base and blade root. The coordinate system for tower loads analysis is a right-handed Cartesian system in which the  $X_T Y_T$  plane is horizontal with the  $X_T$ -axis pointing to the south, the  $Y_T$ -axis pointing to the east, and the  $Z_T$ -axis pointing vertically upwards. The origin of the coordinate system lies where the tower center line intersects the  $X_T Y_T$  plane. Analogously, the coordinate system for blade root loads analysis is a right-handed Cartesian system in which the  $Z_B$ -axis points to the tip along the axis of the blade, the  $X_B$ -axis is perpendicular to the  $Z_B$ -axis and points downward, and the  $Y_B$ -axis is perpendicular to the  $Z_B X_B$  plane. The origin of the coordinate system lies in the center of the blade root. Both coordinate systems are depicted in Figure 7.

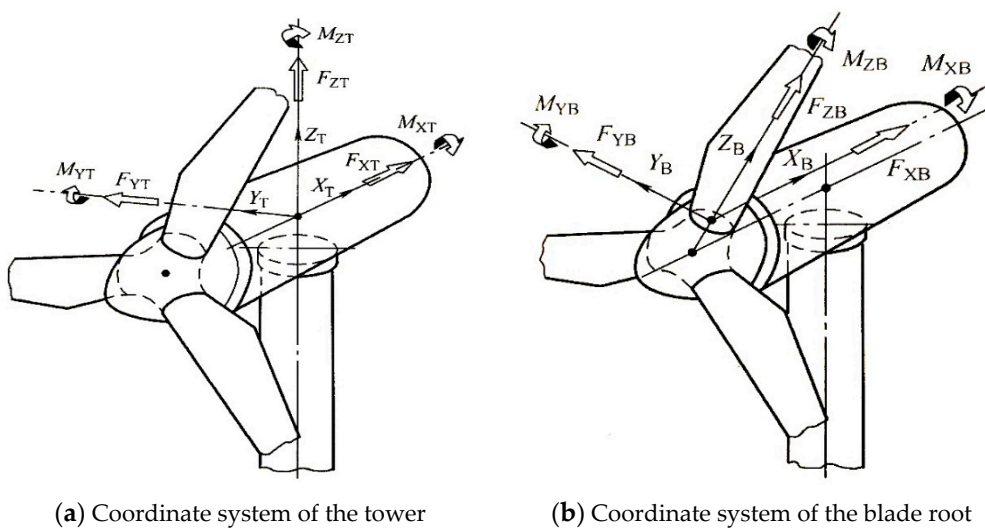
In Figure 7,  $M_{ij}$  is the moment of  $j$  in the  $i$ -axis direction, and  $F_{ij}$  is the force of  $j$  in the  $i$ -axis direction. When  $i$  is X (Y, Z), it refers to the X (Y, Z)-axis. When  $j$  is T (B), it refers to the tower (blade root).



(a) Normal turbulent wind conditions

(b) Extreme turbulent wind conditions

Figure 6. Longitudinal wind speed.



(a) Coordinate system of the tower

(b) Coordinate system of the blade root

Figure 7. Coordinate systems for wind turbine loads analysis.

Rain flow counting methods, which are used in GH Bladed software, process the simulated load time series over all turbine components to determine the damage equivalent loads [37,38], which are thus defined as:

$$S_{eq} = \left( \sum \frac{n_i S_i^m}{N_{eq}} \right)^{1/m} \tag{28}$$

where  $n_i$  is the number of cycles at a load/stress of  $S_i$ ,  $m$  is the S–N curve slope of the component material,  $S_{eq}$  is the damage equivalent loads, and  $N_{eq}$  is the characteristic number of cumulative cycles in 20 years of operation assuming a Rayleigh annual mean wind speed distribution.

The ultimate loads calculation, which is often required for certification calculations, is simple in concept; the results of a load case simulation are analyzed to find the times at which each of a number of specified loads reaches its maximum and minimum values.

According to (28), the number of cycles at load plays a vital role in the calculation of fatigue loads. Normal turbulent wind conditions are one of the most general wind conditions, and fatigue loads should be calculated in these conditions. In addition, ultimate loads are bound to show up in extreme wind conditions, such as extreme turbulent wind conditions. Like wind turbine loads analysis, the frequency of electrical energy fluctuation was analyzed under normal turbulent wind conditions, and the amplitude of electrical energy fluctuation was analyzed under extreme turbulent wind conditions.

## 5.2. Analysis of Simulation Results under Normal Turbulent Wind Conditions

Figure 8 presents the power and pitch rate under the normal turbulent wind conditions obtained via simulation. According to (29), Table 4 lists the values and percentage reduction of the standard deviation (SD) of power and pitch rate.

$$\sigma(x) = \sqrt{\frac{1}{N} \sum_{i=1}^N (x_i - \bar{x})^2} \quad (29)$$

where  $\sigma(x)$  is the SD of data  $x$ ,  $N$  is the quantity of data  $x$ ,  $\bar{x}$  is the average value of data  $x$ , and  $x_i$  is the value of the  $i$ -th number in data  $x$ .

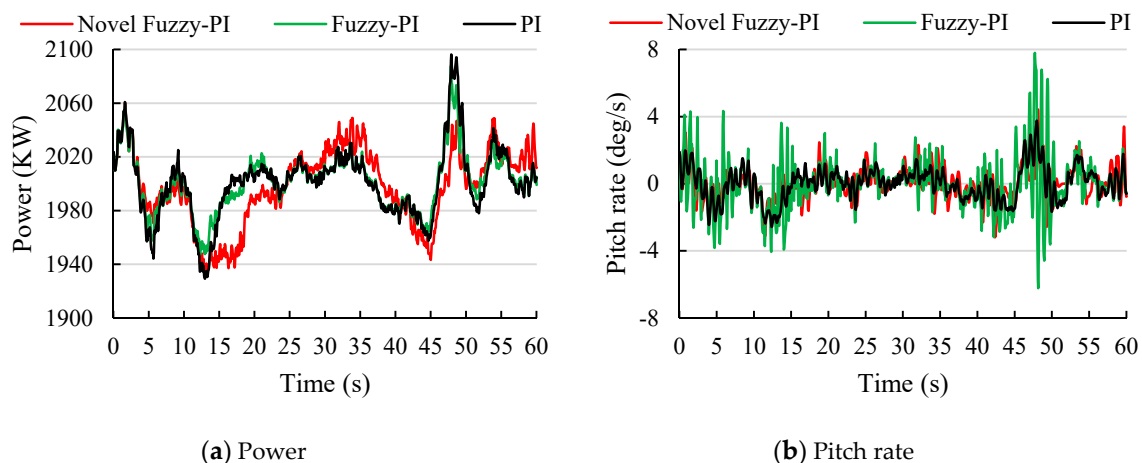


**Figure 8.** The simulation results under normal turbulent wind conditions.

**Table 4.** Analysis of simulation results under normal turbulent wind conditions.

Control Algorithm	SD of Power		SD of Pitch Rate	
	Value (KW)	Variation Compared with PI Control (%)	Value (deg·s <sup>-1</sup> )	Variation Compared with PI Control (%)
PI	26.00	0.00	1.00	0.00
Fuzzy-PI	21.59	−16.96	1.57	+57.00
Novel Fuzzy-PI	28.32	+8.92	0.98	−2.00

These obtained values can be interpreted as follows. By means of the Fuzzy-PI control, compared with PI control, a variation of  $-16.96\%$  in the SD of power and a variation of  $+57.00\%$  in the SD of pitch rate were recorded. These changing amounts in the SDs of power and pitch rate testify that the Fuzzy-PI control can reduce the SD of power, which will reduce the frequency of electrical energy fluctuation. However, it can greatly increase the SD of pitch rate, which will severely increase the fatigue loads of the pitch driver. In addition, compared with PI control, a variation of  $+8.92\%$  in the SD of power and a variation of  $-2.00\%$  in the SD of pitch rate were recorded via the novel Fuzzy-PI control. These changes in the SD of power and pitch rate indicate that the novel Fuzzy-PI control will increase the SD of power, which will increase the frequency of electrical energy fluctuation. However, it can greatly reduce the SD of pitch rate, which effectively solves the problem of large fatigue loads of the pitch driver.

Figure 9 presents the SD values of the moments of the tower base and blade root under the normal turbulent wind conditions obtained via simulation. The percentage improvements of fatigue loads are listed in Table 5. These obtained values could be interpreted as follows. By means of novel Fuzzy-PI control, compared with PI control in terms of fatigue loads of the tower base, improvements of  $9.76\%$  in  $M_{XT}$ ,  $21.53\%$  in  $M_{YT}$ , and  $17.66\%$  in  $M_{XYT}$  were made; by means of Fuzzy-PI control, these values are  $2.78\%$ ,  $15.64\%$ , and  $12.98\%$ , respectively. These improvement percentages in the fatigue loads of the tower base  $M_{XT}$ ,  $M_{YT}$ , and  $M_{XYT}$  demonstrate that, compared with PI control, Fuzzy-PI control

can effectively reduce these fatigue loads, while the novel Fuzzy-PI control can perform even better. In addition, compared with these loads, there was no significant change in the fatigue loads of the blade root and other fatigue loads of the tower base.

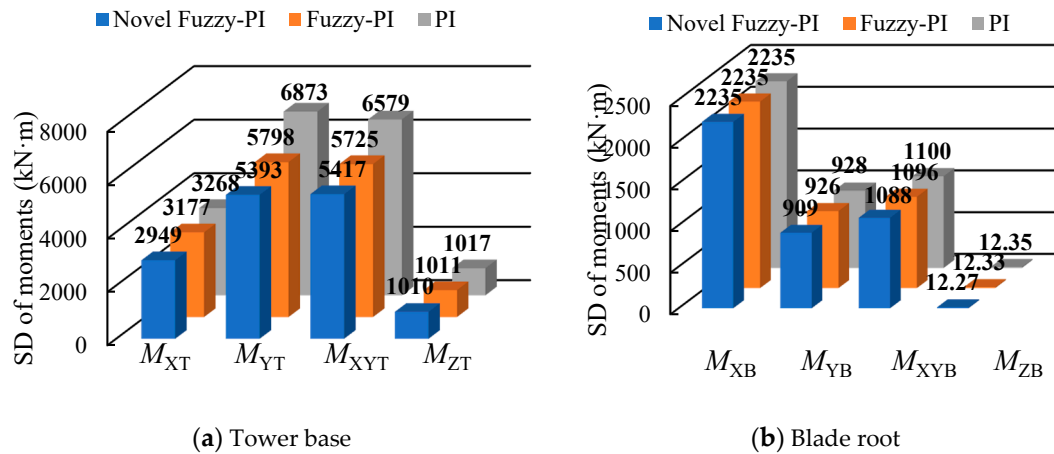


Figure 9. Moments under normal turbulent wind conditions.

Table 5. Analysis of fatigue loads under normal turbulent wind conditions.

Location	Category	Improvement Compared with PI Control (%)	
		Using Novel Fuzzy-PI Control	Using Fuzzy-PI Control
Fatigue loads of tower base	$M_{XT}$	9.76	2.78
	$M_{YT}$	21.53	15.64
	$M_{XYT}$	17.66	12.98
	$M_{ZT}$	0.69	0.59
Fatigue loads of blade root	$M_{XB}$	0.00	0.00
	$M_{YB}$	2.05	0.22
	$M_{XYB}$	1.09	0.36
	$M_{ZB}$	0.65	0.16

### 5.3. Analysis of Simulation Results under Extreme Turbulent Wind Conditions

Figure 10 presents the power and pitch rate under extreme turbulent wind conditions obtained via simulation. According to (30), Table 6 lists the values and percentage variation of the maximum of absolute value (MOAV) of power deviation compared with the rated power and pitch rate.

$$MOAV(x) = \max_{1 \leq i \leq N} (|x_i|) \tag{30}$$

where  $MOAV(x)$  is the maximum of the absolute value of data  $x$ ,  $N$  is the quantity of data  $x$ , and  $x_i$  is the value of the  $i$ -th number in data  $x$ .

These obtained values can be interpreted as follows. By means of the Fuzzy-PI control, compared with PI control, variations of  $-23.26\%$  in the MOAV of power deviation and  $+126.30\%$  in the MOAV of pitch rate were recorded. In addition, compared with PI control, variations of  $-33.86\%$  in the MOAV of power deviation and  $+8.33\%$  in the MOAV of pitch rate were recorded by the novel Fuzzy-PI control. These changes under Fuzzy-PI control demonstrate that it can reduce the MOAV of power deviation, which will reduce the amplitude of electric energy fluctuation, and will greatly increase the MOAV of pitch rate, which will severely increase the ultimate loads of the pitch driver. However, these changes under the novel Fuzzy-PI control indicate that it not only effectively solves the problem of the increasing of the ultimate loads of the pitch driver, but also better reduces the MOAV of power deviation.

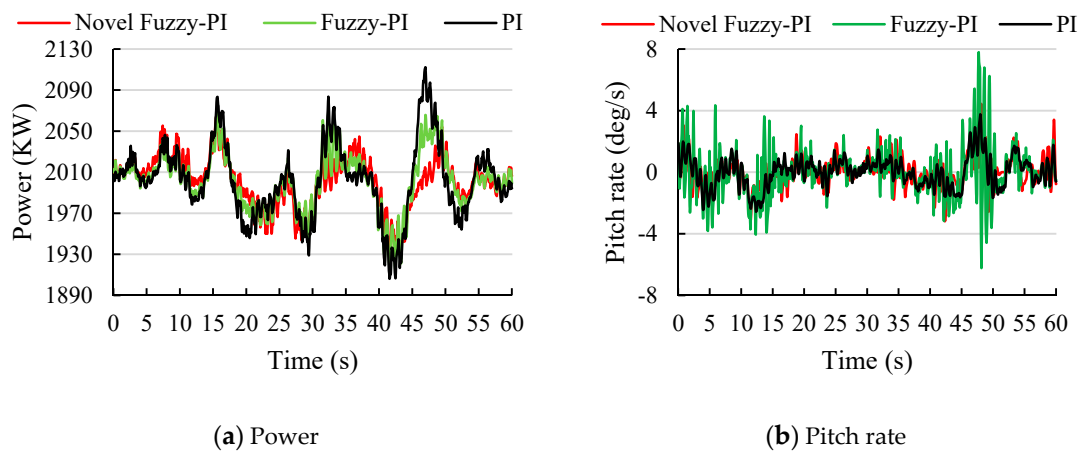


Figure 10. The simulation results under extreme turbulent wind conditions.

Table 6. Analysis of simulation results under extreme turbulent wind conditions.

Control Algorithm	MOAV of Power Deviation Compared with Rated Power		MOAV of Pitch Rate	
	Value (KW)	Variation Compared with PI Control (%)	Value (deg·s <sup>-1</sup> )	Variation Compared with PI Control (%)
PI	112.27	0.00	5.40	0.00
Fuzzy-PI	86.16	-23.26	12.22	+126.30
Novel Fuzzy-PI	74.26	-33.86	5.85	+8.33

Figure 11 presents the MOAV of the moments of the tower base and blade root under extreme turbulent wind conditions obtained via simulation. The percentage improvement of ultimate loads is indicated in Table 7. These obtained values can be interpreted as follows. By means of novel Fuzzy-PI control, compared with PI control in terms of ultimate loads of tower base and blade root, improvements of 18.14% in  $M_{YT}$ , 18.04% in  $M_{XYT}$ , 10.11% in  $M_{YB}$ , and 6.21% in  $M_{XYB}$  were recorded; by means of Fuzzy-PI control, these values are 13.22%, 13.88%, 3.87%, and 2.80%, respectively. These improvement percentages in the ultimate loads of the tower base  $M_{YT}$  and  $M_{XYT}$ , and of the blade root  $M_{YB}$  and  $M_{XYB}$ , demonstrate that, compared with PI control, Fuzzy-PI control can effectively reduce these ultimate loads, while the novel Fuzzy-PI control can perform even better. In addition, compared with these loads, there was no significant change in the other ultimate loads of the tower base and blade root.

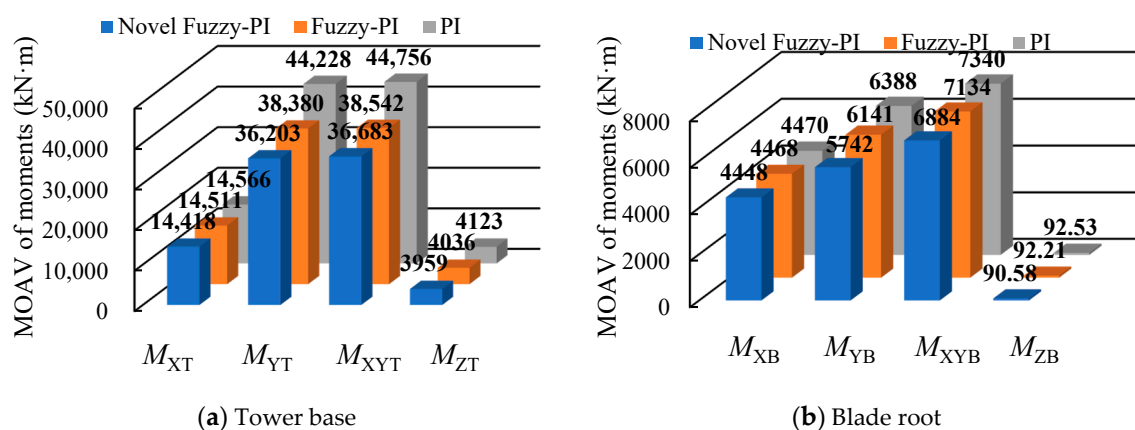


Figure 11. Moments under extreme turbulent wind conditions.

**Table 7.** Analysis of ultimate loads under extreme turbulent wind conditions.

Location	Category	Improvement Compared with PI Control (%)	
		Using Novel Fuzzy-PI Control	Using Fuzzy-PI Control
Ultimate loads of tower base	$M_{XT}$	1.02	0.37
	$M_{YT}$	18.14	13.22
	$M_{XYT}$	18.04	13.88
	$M_{ZT}$	3.98	2.11
	$M_{XB}$	0.49	0.04
Ultimate loads of blade root	$M_{YB}$	10.11	3.87
	$M_{XYB}$	6.21	2.80
	$M_{ZB}$	2.11	0.35

#### 5.4. Discussion

Under the normal and extreme turbulent wind conditions, both of the normal Fuzzy-PI control and the novel Fuzzy-PI control have obvious advantages in load reduction of the tower base and the blade root. In particular, the novel Fuzzy-PI control can reduce these loads by up to 21.53% under the normal turbulent wind condition and by up to 18.14% under the extreme turbulent wind condition. However, the normal Fuzzy-PI control greatly increases the SD of pitch rate, which will severely increase the fatigue loads of the pitch driver. Aiming at the shortcomings of the normal Fuzzy-PI control, a low pass filter is introduced in the novel Fuzzy-PI control after the proportional output item to achieve smooth transition, and then the novel Fuzzy-PI control can effectively reduce the fatigue and ultimate loads of the pitch driver.

#### 6. Conclusions

An improved approach was introduced into the normal Fuzzy-PI control strategy by dividing the fuzzy rules into four areas and analyzing the design method for each area. The study demonstrated that the novel Fuzzy-PI control provided reduced amplitudes of electrical energy fluctuations compared to the normal PI control, while providing slightly higher frequency of these fluctuations. Moreover, the novel Fuzzy-PI control can effectively reduce the fatigue and ultimate loads of the pitch driver, which are introduced by the normal Fuzzy-PI control, through presenting the well-controlled variations of the SD (+57% to −2%) and the MOAV (+126% to +8%) of the pitch rates using the novel Fuzzy-PI control. Furthermore, the study showed that, under the normal turbulent wind condition, the normal Fuzzy-PI control can reduce the fatigue and ultimate loads of the tower base by up to 15.64% while the novel Fuzzy-PI control can further reduce these loads by up to 21.53%; under the extreme turbulent wind condition, the normal Fuzzy-PI control can reduce the fatigue and ultimate loads of the tower base by up to 13.88% while the novel Fuzzy-PI control can further reduce these loads by up to 18.14%. This novel Fuzzy-PI control approach will offer valuable references to the design of the fuzzy rules and the applications in the wind industry.

Due to the adverse offshore wind condition, Ultimate loads of offshore wind turbines are larger while the proposed novel Fuzzy-PI control performs well in reducing ultimate loads. Therefore, in the future works, this novel Fuzzy-PI control can be used to solve this problem while how to set the vital parameters according to the complex offshore wind conditions needs further study, and the study on the application of some statistical approaches can also be carried out.

**Author Contributions:** B.X. and P.J. ran the codes and prepared this manuscript under the guidance of X.S. and Z.G., X.C., Y.Y. and H.L. supervised the work and contributed in the interpretation of the results. All authors carried out data analysis, discussed the results, and contributed to writing the paper. All authors have read and agreed to the published version of the manuscript.

**Funding:** This research was funded by the Fundamental Research Funds for the Central Universities (grant number 2019B14614); the Royal Society Grant IEC/NSFC/19140.

**Conflicts of Interest:** The authors declare no conflict of interest.

## References

1. Rezaeiha, A.; Pereira, R.; Kotsonis, M. Fluctuations of angle of attack and lift coefficient and the resultant fatigue loads for a large Horizontal Axis Wind turbine. *Renew. Energy* **2017**, *114*, 904–916. [[CrossRef](#)]
2. Lin, Y.; Tu, L.; Liu, H.; Li, W. Fault analysis of wind turbines in China. *Renew. Sustain. Energy Rev.* **2016**, *55*, 482–490. [[CrossRef](#)]
3. Akbarimajd, A.; Olyaei, M.; Sobhani, B.; Shayeghi, H. Nonlinear Multi-Agent Optimal Load Frequency Control Based on Feedback Linearization of Wind Turbines. *IEEE Trans. Sustain. Energy* **2018**, *10*, 66–74. [[CrossRef](#)]
4. Tiwari, R.; Babu, N.R.; Sanjeevikumar, P.; Sengupta, S.; Zobaa, A.F.; Sherpa, K.S.; Bhoi, A.K. Fuzzy Logic-Based Pitch Angle Controller for PMSG-Based Wind Energy Conversion System. *Lect. Notes Electr. Eng.* **2017**, *435*, 277–286.
5. Han, B.; Yang, F.; Xiang, Z.; Zhou, L. Individual pitch controller based on fuzzy logic control for wind turbine load mitigation. *IET Renew. Power Gener.* **2016**, *10*, 687–693. [[CrossRef](#)]
6. Van, T.L.; Nguyen, T.H.; Lee, D.-C. Advanced Pitch Angle Control Based on Fuzzy Logic for Variable-Speed Wind Turbine Systems. *IEEE Trans. Energy Convers.* **2015**, *30*, 578–587. [[CrossRef](#)]
7. Civelek, Z.; Luy, M.; Çam, E.; Mamur, H. A new fuzzy logic proportional controller approach applied to individual pitch angle for wind turbine load mitigation. *Renew. Energy* **2017**, *111*, 708–717. [[CrossRef](#)]
8. Tang, K.; Man, K.F.; Chen, G.; Kwong, S. An optimal fuzzy PID controller. *IEEE Trans. Ind. Electron.* **2001**, *48*, 757–765. [[CrossRef](#)]
9. Li, C.; Mao, Y.; Zhou, J.; Zhang, N.; An, X. Design of a fuzzy-PID controller for a nonlinear hydraulic turbine governing system by using a novel gravitational search algorithm based on Cauchy mutation and mass weighting. *Appl. Soft Comput.* **2017**, *52*, 290–305. [[CrossRef](#)]
10. Hamane, B.; Benghanemm, M.; Bouzid, A.; Belabbes, A.; Bouhamida, M.; Draou, A. Control for Variable Speed Wind Turbine Driving a Doubly Fed Induction Generator using Fuzzy-PI Control. *Energy Procedia* **2012**, *18*, 476–485. [[CrossRef](#)]
11. Qi, Y.; Meng, Q. The Application of Fuzzy PID Control in Pitch Wind Turbine. *Energy Procedia* **2012**, *16*, 1635–1641. [[CrossRef](#)]
12. Hamane, B.; Doumbia, M.L.; Bouhamida, M.; Benghanem, M. Control of wind turbine based on DFIG using Fuzzy-PI and Sliding Mode controllers. In Proceedings of the Ninth International Conference on Ecological Vehicles and Renewable Energies, Monte Carlo, Monaco, 25–27 March 2014.
13. Civelek, Z.; Luy, M.; Cam, E.; Barışçı, N.; Barışçı, N. Control of Pitch Angle of Wind Turbine by Fuzzy Pid Controller. *Intell. Autom. Soft Comput.* **2015**, *22*, 463–471. [[CrossRef](#)]
14. Sarafraz, M.; Tlili, I.; Tian, Z.; Bakouri, M.; Safaei, M.R. Smart optimization of a thermosyphon heat pipe for an evacuated tube solar collector using response surface methodology (RSM). *Phys. A Stat. Mech. Appl.* **2019**, *534*, 122–146. [[CrossRef](#)]
15. Sarafraz, M.; Safaei, M.R.; Goodarzi, M.; Arjomandi, M. Experimental investigation and performance optimisation of a catalytic reforming micro-reactor using response surface methodology. *Energy Convers. Manag.* **2019**, *199*, 111983. [[CrossRef](#)]
16. Li, Z.; Renault, F.L.; Gómez, A.O.C.; Sarafraz, M.; Khan, H.; Safaei, M.R.; Filho, E.P.B. Nanofluids as secondary fluid in the refrigeration system: Experimental data, regression, ANFIS, and NN modeling. *Int. J. Heat Mass Transf.* **2019**, *144*, 118635. [[CrossRef](#)]
17. Liu, J.; Gao, Y.; Geng, S.; Wu, L. Nonlinear Control of Variable Speed Wind Turbines via Fuzzy Techniques. *IEEE Access* **2016**, *5*, 27–34. [[CrossRef](#)]
18. Jonkman, J.M.; Butterfield, S.P.; Musial, W.D.; Scott, G.W. *Definition of a 5-MW Reference Wind Turbine for Offshore System Development*; Office of Scientific & Technical Information Technical Reports; National Renewable Energy Lab. (NREL): Golden, CO, USA, 2009.
19. Habibi, H.; Koma, A.Y.; Sharifian, A. Power and velocity control of wind turbines by adaptive fuzzy controller during full load operation. *Iranian J. Fuzzy Syst.* **2016**, *13*, 35–48.
20. Habibi, H.; Nohooji, H.R.; Howard, I. Adaptive PID Control of Wind Turbines for Power Regulation with Unknown Control Direction and Actuator Faults. *IEEE Access* **2018**, *6*, 37464–37479. [[CrossRef](#)]

21. Habibi, H.; Howard, I.; Simani, S. Reliability improvement of wind turbine power generation using model-based fault detection and fault tolerant control: A review. *Renew. Energy* **2019**, *135*, 877–896. [[CrossRef](#)]
22. Asgharnia, A.; Shahnazi, R.; Jamali, A. Performance and robustness of optimal fractional fuzzy PID controllers for pitch control of a wind turbine using chaotic optimization algorithms. *ISA Trans.* **2018**, *79*, 27–44. [[CrossRef](#)]
23. Mehrpooya, M.; Hejazi, S. Design and Implementation of Optimized Fuzzy Logic Controller for a Nonlinear Dynamic Industrial Plant Using Hysys and Matlab Simulation Packages. *Ind. Eng. Chem. Res.* **2015**, *54*, 11097–11105. [[CrossRef](#)]
24. Cervantes, L.; Castillo, O. Type-2 fuzzy logic aggregation of multiple fuzzy controllers for airplane flight control. *Inf. Sci.* **2015**, *324*, 247–256. [[CrossRef](#)]
25. Meng, W.; Yang, Q.; Ying, Y.; Sun, Y.; Yang, Z.; Sun, Y. Adaptive Power Capture Control of Variable-Speed Wind Energy Conversion Systems with Guaranteed Transient and Steady-State Performance. *IEEE Trans. Energy Convers.* **2013**, *28*, 716–725. [[CrossRef](#)]
26. Ang, K.H.; Chong, G.; Li, Y. PID control system analysis, design, and technology. *IEEE Trans. Control. Syst. Technol.* **2005**, *13*, 559–576.
27. Hassairi, W.; Bousselmi, M.; Abid, M.; Sakuyama, C.V. Notice of Violation of IEEE Publication Principles: Using matlab and Simulink in SystemC verification environment by JPEG algorithm. In Proceedings of the 16th IEEE International Conference on Electronics, Circuits and Systems, Yasmine Hammamet, Tunisia, 13 December 2009.
28. Blair, W.; Joao, L.D.M.; Davis, L.; Anderson, P. Streamlining the Genomics Processing Pipeline via Named Pipes and Persistent Spark Satasets. In Proceedings of the 17th IEEE International Conference on Bioinformatics & Bioengineering, Herndon, VA, USA, 23 October 2017.
29. Zhu, Q.; Qiu, B. Research on Trajectory Tracking Control of Aircraft in Carrier Landing. In Proceedings of the Third International Conference on Instrumentation, Measurement, Computer, Communication and Control, Shenyang, China, 21 September 2013.
30. Simani, S.; Castaldi, P. Active actuator fault-tolerant control of a wind turbine benchmark model. *Int. J. Robust Nonlinear Control.* **2013**, *24*, 1283–1303. [[CrossRef](#)]
31. He, W.; Ge, S.S. Vibration Control of a Nonuniform Wind Turbine Tower via Disturbance Observer. *IEEE/ASME Trans. Mechatron.* **2015**, *20*, 237–244. [[CrossRef](#)]
32. Yin, M.; Li, W.; Chung, C.Y.; Chen, Z.; Zou, Y. Inertia compensation scheme of WTS considering time delay for emulating large-inertia turbines. *IET Renew. Power Gener.* **2017**, *11*, 529–538. [[CrossRef](#)]
33. Aho, J.; Bucksapan, A.; Laks, J.; Jeong, Y.; Dunne, F.; Pao, L. A tutorial of wind turbine control for supporting grid frequency through active power control. In Proceedings of the 2012 American Control Conference, Montreal, QC, Canada, 27 June 2012.
34. Kaimal, J.C.; Wyngaard, J.C.; Izumi, Y. Spectral characteristics of surface-layer turbulence. *Q. J. R. Meteorol. Soc.* **1972**, *98*, 563–589. [[CrossRef](#)]
35. Von Karman, T. Progress in the Statistical Theory of Turbulence. *Proc. Natl. Acad. Sci. USA* **1948**, *34*, 530–539. [[CrossRef](#)]
36. International Electrotechnical Commission, International Standard. *IEC 61400-1 Wind Turbines—Part 1: Design Requirements*, 3rd ed.; International Electrotechnical Commission: Geneva, Switzerland, 2005.
37. Zhao, H.; Wu, Q.; Huang, S.; Yan, M.; Yang, Y.; Sun, H. Fatigue Load Sensitivity-Based Optimal Active Power Dispatch for Wind Farms. *IEEE Trans. Sustain. Energy* **2017**, *8*, 1247–1259. [[CrossRef](#)]
38. Berg, J.; Natarajan, A.; Mann, J.; Patton, E.G. Gaussian vs non-Gaussian turbulence: Impact on wind turbine loads. *Wind. Energy* **2016**, *19*, 1975–1989. [[CrossRef](#)]

**Publisher’s Note:** MDPI stays neutral with regard to jurisdictional claims in published maps and institutional affiliations.



© 2020 by the authors. Licensee MDPI, Basel, Switzerland. This article is an open access article distributed under the terms and conditions of the Creative Commons Attribution (CC BY) license (<http://creativecommons.org/licenses/by/4.0/>).